Luminescent Silicon Diatom Replicas: Self-Reporting and Degradable Drug Carriers with Biologically Derived Shape for Sustained Delivery of Therapeutics

Shaheer Maher, Mohammed Alsawat, Tushar Kumeria, Dina Fathalla, Gihan Fetih, Abel Santos, Fawzia Habib, and Dusan Losic**

Current development of drug microcarriers is mainly based on spherical shapes, which are not biologically favorable geometries for complex interactions with biological systems. Scalable synthesis of drug carriers with nonspherical and anisotropic shapes featuring sustained drug-releasing performances, biocompatibility, degradability, and sensing capabilities is challenging. These challenges are addressed in this work by employing Nature's optimized designs obtained from low-cost diatomaceous earth mineral derived from single-cell algae diatoms. Silica diatoms with unique shapes and 3D microcapsule morphology are converted into silicon diatom replicas with identical structure by a magnesiothermic reduction process. The results reveal that prepared silicon diatoms have a set of unique properties including favorable microcapsule structure with high surface area and micro/mesoporosity providing high drug loading, fast biodegradability, and intrinsic luminescence, which make them highly suitable for low-cost production of advanced drug microcarriers. Their sustained drug release >30 days combined with self-reporting function based on silicon luminescence properties using nonluminescent and luminescent drugs for intravitreal drug therapy is successfully demonstrated. These silicon diatoms offer promising potential toward scalable production of low-cost and advanced microcarriers for broad medical therapies, including theranostics and microrobotic guided drug delivery devices.

1. Introduction

To advance current drug delivery systems, many materials including polymeric nanoparticles, liposomes, micelles, carbon nanotubes, dendrimers, magnetic nanoparticles, silicon oxide nanoparticles, and quantum dots have been synthetized and explored as drug carriers for delivery of therapeutics.[1] Although some of these delivery systems have been commercialized or are in clinical trials, a broader translation of these materials into real clinical applications suffers from many hindrances.[2,3] Particle size and surface chemistry are the most important parameters of these drug carriers that have been studied to understand their function and improve the performance.[4] Surprisingly, the shape of the particles was not considered to be a critical parameter that affects the biological interactions of such drug carriers. However, there are a growing number of recent studies showing that particle shape and geometry plays a significant role in these interactions including transport through the blood vessels and organs, internalization into cells, and targeting diseased sites.[5–7] The effect of the shape was reasonable to consider based on the fact that a majority of entities in the biological systems are not a spherical shape. Unusual shapes at micro and nanoscale such as elliptical, rods, tubes, bullets, spiral, etc. are adapted by most microorganisms including viruses and bacteria providing them unique biological functions and advantages.[8,9] The synthesis of micro and nanoparticles with nonspherical and anisotropic shapes as drug carriers to mimic some of these functions has been addressed using a variety of fabrication methods including self-assembly, photolithography, template molding, and microfluidics.[10,11] However, these methods are based on high-cost materials and the use of expensive equipment, which makes the large-scale production of these types of drug carriers not sustainable and commercially feasible.

To address these disadvantages, Nature generated peculiar shapes of biological origin optimized through evolution of biological interactions offers an unprecedented source of natural materials for the production of these shape-optimized drug carriers. Single-celled algae microorganisms, called diatoms, are the most spectacular example of biologically evolved materials with micro and nanoscale dimensions with unmatchable variation of shapes and nanostructural features of their

S. Maher, M. Alsawat, Dr. T. Kumeria, Dr. A. Santos, Prof. D. Losic
School of Chemical Engineering
The University of Adelaide
Engineering North Building, 5005 Adelaide, Australia
E-mail: abel.santos@adelaide.edu.au; dusan.losic@adelaide.edu.au
S. Maher, Dr. D. Fathalla, Dr. G. Fetih, Prof. F. Habib
Faculty of Pharmacy
Assiut University
71526 Assiut, Egypt

DOI: 10.1002/adfm.201501249

exoskeletons (frustules) built by amorphous silica.[12–15] Each of the estimated 10^5 diatom species has a specific frustule shape decorated with a unique pattern of nanosized features such as pores, ridges, and spines with specific functions and properties that are optimized for movement and interactions in a complex biological environment.[12,13] Their hollow pill-box structure, aerodynamic shape with a variety of sizes (500 nm to 50 µm), large inner space with micro and nanoscale porosity, high surface area, high permeability, and proved biocompatibility make diatoms a promising carrier to overcome the shape challenges of existing synthetic microparticle delivery systems.[15,16] More importantly, diatoms are natural material that can be easily cultivated or supplied in large quantities from diatomite or diatomaceous earth (DE) mineral (fossilized diatoms) available in millions of tons as a low-cost commodity from the mining industry. In our previous work, we demonstrated for the first time that diatoms can be used as drug carriers showing a new concept of magnetically guided microcarriers for drug delivery based on functionalized diatom by dopamine-modified iron oxide nanoparticles.[17–22] Diatom silica is proved as a biocompatible material and used in the food and medical supplement industry; however, it suffers from poor biodegradability which is a major problem for its drug delivery applications. In this study, we address this problem by converting diatom silica into degradable silicon replicas and explore their capabilities and properties as sustained and self-reporting drug carriers relevant for intraocular therapy.

There is an urgent need for drug delivery systems with controlled and sustained drug release that can be easily monitored to treat intraocular diseases affecting the retina and choroid such as choroidal neovascularization (CNV) in age-related macular degeneration (ARMD) and proliferative vitreoretinopathy (PVR).[23] A local drug administration of intravitreal drugs has become a standard medical practice, but has many adverse side effects since drug must be frequently administered due to the short half-life of available drugs (e.g., daunorubicin (DNR), 131 min, which means one intravitreal injection every four hours). This may lead to mechanical damage of tissues, hemorrhage, lens dislocation, and increased risk of infection (i.e., up to 1%, which could lead to visual loss), making this therapy less patient compliant and expensive. In that respect, more advanced localized drug delivery systems are required which are able to provide sustained drug release locally where degradable microcarriers are recognized as a promising solution.[24–26] Recently, drug carriers based on porous silicon (pSi) microparticles prepared by electrochemical etching of silicon have been extensively explored to treat ocular diseases. The pSi microparticles as drug carriers have a high surface area, biocompatibility, and biodegradability and can be engineered in order to produce photonic crystals, which make it possible to monitor the loading and release of therapeutic agents.[27–34] However, the scalability of the fabrication process of pSi particles is challenging, since it involves several electrochemical etching steps using highly toxic chemicals such as hydrofluric acid (HF), which require specific safety precautions. Moreover, the use of HF during the synthesis process of pSi may eventually lead to residual toxicity in pSi microparticles, limiting the applicability of this system for real medical treatments.[35] Another limitations of these pSi drug carriers for in vivo self-reporting intraocular drug delivery are due to the fluidic nature of the eye vitreous and the angle-dependent photonic properties of pSi (i.e., the spectrum and color of pSi particles rely not only on the amount of drug loaded/released but also on the angle of incidence of light).[36,37] This limitation, however, could be overcome by developing luminescent drug carriers with shaped morphology and angle-independent optical properties.

In this context, we present this study aimed to demonstrate the applicability of silicon diatoms converted from silica diatoms as new drug delivery microcarriers with biologically derived shapes. Our approach is depicted in **Scheme 1** describing the silica to silicon diatoms conversion process, drug-loading, drug

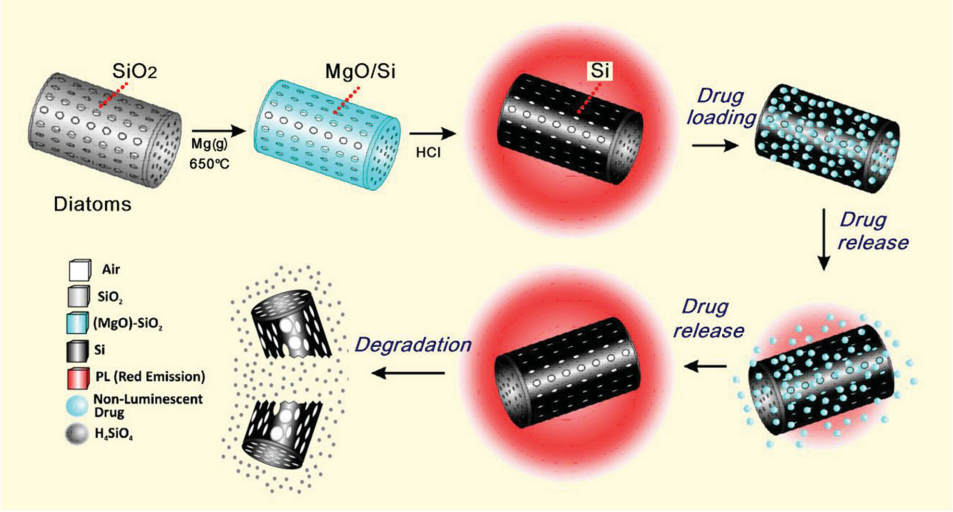

Scheme 1. Schematic illustration of the gas/silica displacement method based on the magnesiothermic reduction process employed to convert silica diatoms 3D structure into luminescent silicon replicas as a new biodegradable microcarrier with self-reporting function with unique biological-derived shape desirable for high drug loading and sustainable release for broad drug delivery applications.

release, self-reporting, and degradation of these new silicon microcarriers. The first objective of this work is to demonstrate the preparation of silicon replicas with diatom morphology from low-cost DE natural material by adapting the existing magnesiothermic reduction process followed by the characterization of their chemical, structural, and optical properties relevant to drug loading/delivery and sensing performance. Our second objective is to evaluate the biodegradability of prepared silicon diatoms by studying their in vitro degradability under physiological conditions, which is one of the critical parameters for drug delivery applications of microcarriers. Third objective is to demonstrate their two outstanding features: 1) sustained drug release based on its unique biologically derived microcapsule structure and mesoporosity and 2) self-reporting functions based on the intrinsic luminescence properties of silicon replicas which are evaluated by drug release of daunorubicin (luminescent therapeutic agent) and indomethacin (nonluminescent therapeutic agent). Significance and potential application of silicon diatoms microcarriers for intraocular therapy is finally explored by in vitro drug delivery experiment to define their sustained drug release and degradation behavior.

2. Results and Discussion

2.1. Structural, Morphological, and Chemical Characterization

Typical morphology and structural details of silica and silicon diatoms obtained from purified DE material are presented by scanning electron microscopy (SEM) images in **Figure 1**a–c and Figure S1 (Supporting Information). Several different centric diatom species were identified in DE material and *Aulacoseira sp*. originated from the fresh waters is determined as the major species (>90%). These diatoms have characteristic 3D cylindrical porous structures with diameters of 6.25 ± 0.85 µm, length 12 ± 4.5 µm, the wall thickness of 300 ± 20 nm (as measured by SEM), and regularly spaced rows of larger pores (400 ± 40 nm) and smaller pore (100 ± 20 nm) on the ends (Figure S1, arrows, Supporting Information). They have two types of microcapsule structures, one is full frustule with both ends closed and the second is half frustule with one end closed and one end half open (Figure S1b–d, Supporting Information). By applying a simple and scalable purification method a large quantity of these diatom silica microcapsules can be obtained from low-cost natural DE material.

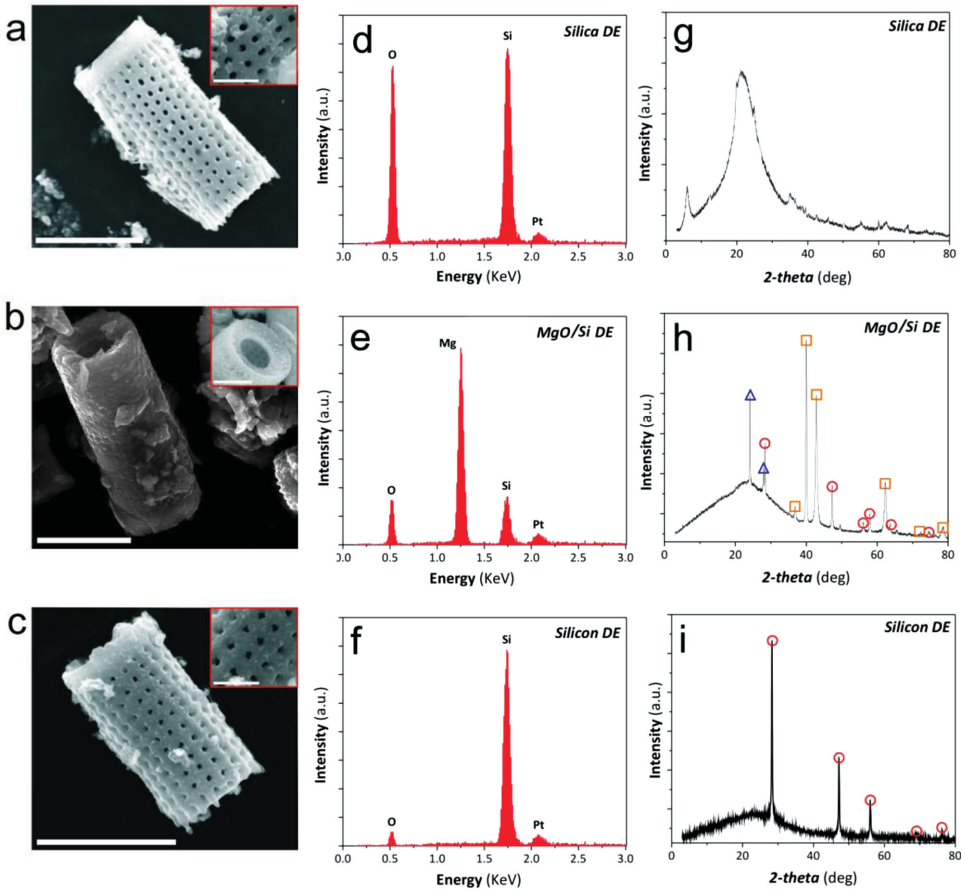

Figure 1. Morphological, structural, and chemical characterization of conversion silica into silicon diatoms replicas using the magnesiothermic reduction process. SEM images showing single diatom structure starting from a) initial silica diatom; b) intermediate product, MgO/Si composite; and c) silicon diatom replica with insets showing high-resolution image pore structures (scale bar for (a), (b), and (c) = 10 µm, insets = 2 µm). d–f) EDX spectra of these stages confirming the successful reduction process evidenced by significant reduction of oxygen and increase of silicon peak in silicon replicas. g–i) XRD patterns showing amorphous structure of initial diatoms, magnesia (□), magnesium orthosilicate traces (△) in MgO/Si intermediate and only silicon (○) peaks reduced silicon replicas.

SEM images representing single diatom structure through all three steps of the magnesiothermic process from initial diatom silica, MgO/Si intermediate to final silicon diatoms is shown in Figure 1a–c confirming no observable changes in their morphology. During this process, the magnesium source was melted and its vapors initiated the redox reaction on the silica diatoms material causing the reduction of silica diatoms (SiO_2) to silicon diatom replicas, which resulted in the production of an intermediate product MgO/Si diatom composite containing magnesia (MgO) (Figure 1b), a by-product that is selectively removed by acid chemical etching (1 M HCl) (Figure 1c). Note that slight increase in surface roughness was observed on high-resolution SEM images of silicon diatoms (Figure 1c, inset, and Figure S2, Supporting Information) as a result of the reduction process. The conversion of silica into silicon is also observable by a color change of the obtained particles, which changed from white color of silica diatoms to dark brown of silicon diatom replicas (Figure S3, Supporting Information).

The chemical composition of silica diatom, MgO/Si intermediate, and silicon diatom replicas were analyzed by energy-dispersive X-ray spectroscopy (EDX), X-ray diffraction (XRD), Fourier transform IR (FTIR) spectroscopy, and Raman spectroscopy. These results confirmed the successful conversion of silica to silicon after the magnesiothermic process. EDX spectrum for silica diatom samples displayed typical peaks for silicon and oxygen, whereas the oxygen peak for silicon diatom replicas was reduced to negligible level (Figure 1d,f), indicating the reduction of the diatom silica structure. EDX also confirmed the complete dissolution of MgO after treatment with HCl (1 M) as the peak for Mg disappeared as compared to silicon/Mg composite diatom replicas (Figure 1e). The lattice structure of diatoms before and after the magnesiothermic reduction reaction was assessed by XRD to further confirm the successful reduction of silica diatoms into silicon diatom replicas (Figure 1g–i). The XRD pattern for diatom silica is mainly composed of amorphous silica as indicated by the amorphous silica peak (broad hump around 20°) with a residual trace of crystalline silicon.[38] In contrast, MgO peaks appeared on the XRD pattern of MgO/silicon composites replicas (Figure 1h) with traces of magnesium orthosilicate (Mg_2O_4Si). Figure 1i displays the XRD pattern of silicon diatom replicas after treating Si/MgO composite replicas with HCl (1 M) to remove MgO and other impurities. This analysis demonstrates that no MgO peaks appear in this XRD spectrum, while sharp crystalline silicon peaks were observed, denoting the crystalline structure of silicon diatom replicas. It is worth noting that treatment with HCl did not affect these converted diatom structures of silicon, as shown in Figure 1i, which are consistent with the aforementioned EDX analysis. Raman spectroscopy data presented in Figure S4 (Supporting Information) denote the appearance of a sharp Raman shift peak at 520 cm^{-1}, which confirms the complete conversion of the diatom silica to crystalline silicon. In contrast, no Raman shift peak was observed for silica diatom structure. Finally, comparative FTIR spectra (Figure S5, Supporting Information) obtained from initial diatom and their silicon replicas confirmed the successful reduction process. Figure S4a (Supporting Information) shows silica diatom spectrum with a strong peak around 1100 cm^{-1} corresponding to stretching mode of Si—O—Si of diatom silica precursor, whereas Figure S4b (Supporting Information) displays vibrations around 2200 cm^{-1}, which is associated with Si—H stretching in the case of silicon diatom replicas.[39]

Nitrogen adsorption/desorption isotherm analysis presented in **Figure 2** revealed that the specific surface area of the silicon diatom replicas increased significantly up to 156 ± 16 $m^2\ g^{-1}$, which is 13-fold higher as compared to their silica initial precursor (12 ± 1 $m^2\ g^{-1}$) used in this work (Figure 2a–c). The specific surface area of the MgO/Si composite network was 6 ± 1 $m^2\ g^{-1}$ (Figure 2b), which is twofold smaller than that of the diatom silica precursor. These results showing significant increased surface area of silicon diatom replicas are in agreement with previous report by Bao et al. and are explained by the increment of specific surface area as the result of the formation of more ordered silicon crystal lattice upon reduction compared to the amorphous silica structure.[40] The BJH (Barrett–Joyner–Halenda) model of N_2 desorption data showed a similar trend in total pore volume (i.e., specific volume) with values of 0.073 ± 0.0012 $cm^3\ g^{-1}$ and 0.05 ± 0.002 $cm^3\ g^{-1}$ for diatom silica and MgO/Si composite, respectively. However, silicon diatom replicas possess a highly porous structure with total pore volume of 0.65 ± 0.023 $cm^3\ g^{-1}$, after the dissolution of MgO with the significantly reduced average mesopore diameter of 13 ± 1 nm compared to 23 ± 3 nm for diatom silica. These considerable changes in specific surface area and mesoporosity of silicon diatom replicas can be explained by the volume changes of silica amorphous structure to silicon crystal structure occurred during the magnesiothermic process. The diatom frustules were made through complex still not well understood genetically guided biosilica morphogenesis through sophisticated 3D self-assembly process in silica deposition vesicle involving transport monomeric silica ($Si(OH)_4$) their nucleation and formation of large silica nanoparticle units (20–50 nm depends of species) which are considered as basic building blocks of diatom structures. These silica nanoparticles were assembled with very strong binding through species specific 3D templating process to make characteristic ordered porous structure of diatom frustule with unprecedented mechanical strength.[41] High-resolution SEM and atomic force microscopy (AFM) images presented in Figure 2d–f clearly indicate the "hillock" topography of the diatom surface which confirms this hypothesis. The scheme of silica nanoparticles as building block of diatom silica structure is presented in Figure 2g to explain the change in specific surface area and porosity associated with the SiO_2 to Si conversion process. These schemes indicate the consequences of reduced volume of converted silica nanoparticles into silicon nanoparticles and the formation of nanovoids between them (Figure 2a–c, insets). However, it is important to state that diatom silicon replicas still have mechanically strong structure and this volume reduction did not cause the collapsing of its 3D structure.

All the above-described characterization steps demonstrate the successful formation of silicon diatoms by the magnesiothermic process. The application of Mg as a reducing agent allowed the use of a moderate temperature (650 °C) for the reduction process to occur. Therefore, at this low temperature Mg catalyst-based reduction process not only makes it possible to achieve a complete conversion of diatom silica into silicon replicas but also to preserve the hierarchical porous structure and morphology of diatoms. In order to adapt the magnesiothermic reduction process more scalable for industrial applications, we recently improved

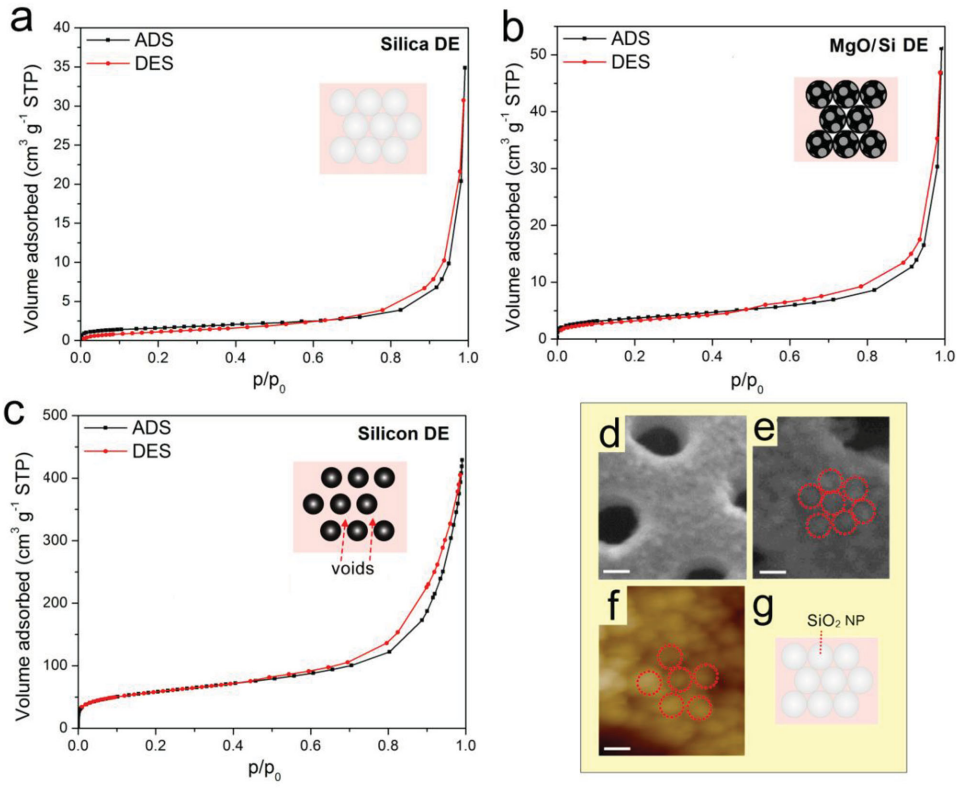

Figure 2. Nitrogen adsorption/desorption isotherms obtained from a) silica diatoms, b) MgO/Si intermediate product, and c) silicon diatoms. The scheme showing changes of silica diatoms building blocks (silica nanoparticles) during the conversion process is presented in insets. d,e) High-resolution SEM images and f) AFM image of diatom silica surface showing typical topography which indicates their silica nanoparticles (SiO_2 NP) composition which are presented schematically in (g).

the original approach using sealed stainless steel ampoules reported by Bao et al.[40,42] Instead, we heated the magnesium (Mg) source and the diatom silica in a ceramic boat inside of a furnace under argon gas flow which does not require a sealed boat/cell design, nor heat scavengers and can be scaled-up.

2.2. In Vitro Degradation of Silicon Diatom Microcapsules

Drug carriers proposed for drug delivery applications should not only provide a sustained and long-lasting release of therapeutic agents but also degrade into nontoxic species that can be incorporated into the living environment without safety issues. This requirement has been successfully achieved by pSi particles-based ocular drug delivery formulations, which degraded in rabbit vitreous within 10 days in the form of silicic acid (H_4SiO_4), without any evident sign of toxicity.[26,43] Poor degradability was one of the major problems for diatom silica microcarriers for drug delivery application as indicated in our previous work.[21,39] To confirm biodegradation properties of prepared silicon diatoms we explored their in vitro degradation behavior under simulated physiological conditions (i.e., phosphate-buffered saline (PBS) at pH 7.4 and 37 °C), which prevail inside the vitreous of the eye. **Figure 3** provides the in vitro dissolution results for silica and silicon diatoms over a period of 30 days obtained by inductively coupled plasma mass spectrometry (ICP-MS) and SEM imaging. The results show, as expected, a significant increase in the rate of degradation of silicon diatoms compared with silica diatoms. From this study, we found that 20% of silicon diatoms dissolved throughout the period of study (i.e., 30 days), whereas diatom silica degraded less than 1% within the same timeframe. Comparative SEM imaging was performed to confirm these structural changes and selected images showing silica and silicon diatoms structure during 10 and 30 days of the degradation process. No changes are observed on silica diatoms during 30 days, and only slight changes on silicon diatoms after 10 days (i.e., macropores became wider as their walls dissolve), but significant changes after 30 days showing one part of silicon structure is totally dissolved, and eventually we expect that silicon diatoms will be totally dissolved. These are highly desirable properties for proposed intraocular applications since vitreous humor of eye has low turnover rate (i.e., constrained blood flow). Therefore, the higher dissolution rate of silicon diatoms is advantageous as it prevents the accumulation of the particles in the vitreous body after treatment and suggests their potential application to treat intraocular diseases.

2.3. Drug Loading and In Vitro Drug Release of Silicon Diatoms

In vitro drug loading and release characteristics of silicon diatoms were assessed using daunorubicin (DNR) as an antiproliferative agent model. DNR is an anthracycline antibiotic which inhibits topoisomerase to prevent RNA and DNA formation inside cells

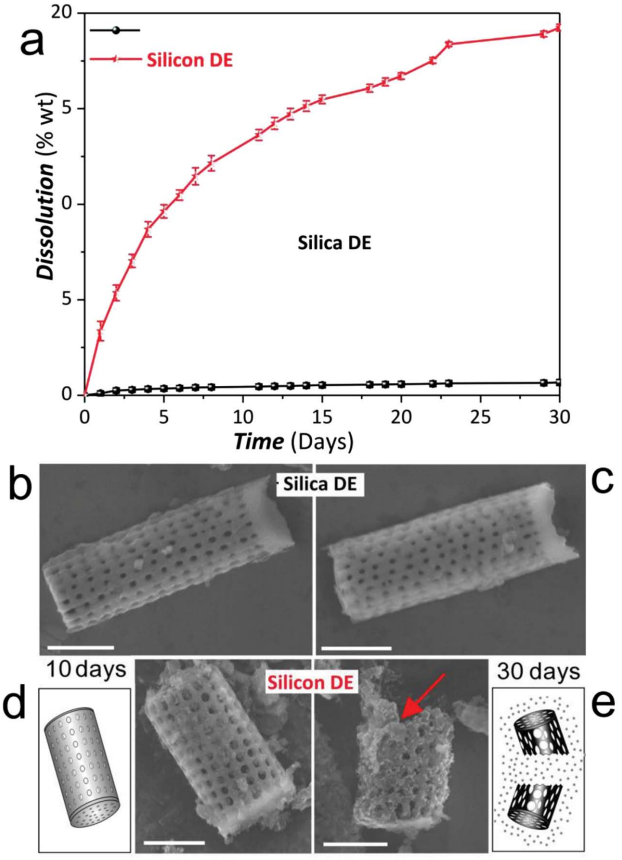

Figure 3. Comparative degradation behavior of silica diatoms and their silicon replicas. a) In vitro degradation in PBS at pH 7.4 showing the percent of silicon (% wt) dissolved. SEM images of b,c) silica diatom and d,e) silicon diatoms replicas after 10 and 30 days of the dissolution process with schematic representation of their degradation process.

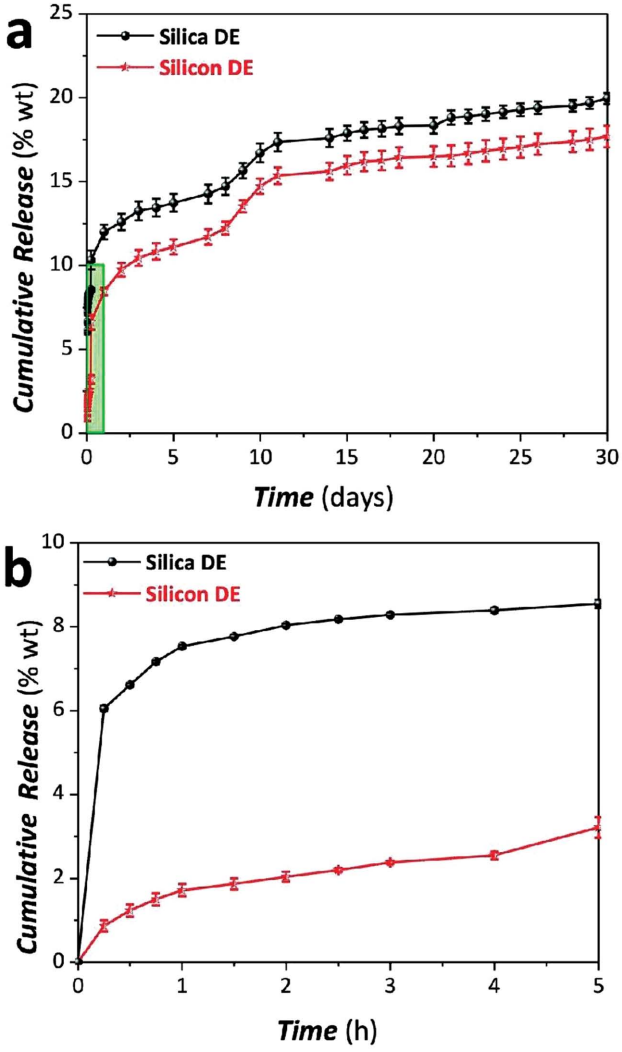

Figure 4. Drug release profiles of model drug daunorubicin (DNR) (luminescent therapeutic agent) showing comparative cumulative release from silica diatoms and their silicon replicas after a) 30 days and b) 5 h (burst release) presenting magnified view of the green rectangle shown in (a).

and is used for treating PVR and other intraocular diseases. However, conventional drug delivery administration of DNR has some inherent limitations, including a short half-life (131 min) in the vitreous, which requires repeated adminstration, and narrow therapeutic index, which may result in cardiac toxicity due to its high water solubility (39.2 μg mL^{-1}).[44–46] The DNR loading capacity (calculated by Equation (1)) of silicon diatoms was found to be 32 ± 0.3 μg mg^{-1}, whereas the control material (i.e., silica diatoms) presented a slightly higher loading capacity (41 ± 0.7 μg mg^{-1}). The higher drug loading capacity of silica diatoms could be due to hydrogen bonding between the primary amine of DNR and hydroxyl groups present on the surface of diatom silica. However, this amount of drug loading in silicon diatoms is comparable or slightly higher than that achieved through physical adsorption onto silicon and silica porous nanoparticles reported in previous studies.[24,47]

The in vitro release of DNR in PBS (at pH 7.4) from silicon diatoms compared with silica diatoms (control) revealed a biphasic elution profile with an initial 5 h long burst release followed by a sustained release over the entire period of study (30 days) (**Figure 4**). Burst release can be attributed to the release of physisorbed drug molecules from the particles surface. The silicon diatoms eluted only about 3% of the loaded drug, whereas the cumulative in vitro release of DNR from the control (i.e., silica diatoms) was almost threefold higher (i.e., >8 %) during the same period of time. This could be due to the large pore volume (i.e., specific volume) of silicon diatoms (0.65 cm^3 g^{-1}), which allowed more drug to be trapped inside the structure as compared to silica diatoms (pore volume 0.073 cm^3 g^{-1}), in which more drug molecules are physisorbed onto the surface. The cumulative DNR release from both the carriers (i.e., silica and silicon diatoms replicas) after 30 days was 19.9 ± 0.3% and 17.6 ± 0.6% of the total loading, respectively. Note that the initial burst release for silicon diatoms is less than half of the release values obtained from silica diatoms, while the total amount of drug released during a 30 days period is almost the same for both the drug carriers. This reveals that the release mechanism of the drug for diatom silica is dominated by the diffusion of the drug molecules through the porous structure due to concentration gradient. On the other hand, the release mechanism in the case of silicon diatom replicas is diffusion controlled at the initial release stage (i.e., burst release

during the first few hours) and subsequently the process is governed by a combination of diffusion and matrix degradation (i.e., degradation of the silicon diatom structure). Note that the therapeutic window of DNR is 1.88–5.64 μg mL^{-1} (i.e., milligrams per milliliter of vitreous humor) throughout the whole administration period.[24] To determine whether our system maintains a sustained release of DNR within the desired therapeutic window, we estimated mathematically the release rate of drug per hour from the aforementioned experimental results (Figure S6, Supporting Information). Our drug release formulation with silicon diatoms can achieve the effective concentration (MEC) of DNR after 5 h (the cumulative amount of drug released within this timeframe was 2 μg mL^{-1}). After reaching this level (i.e., MEC), the amount of drug released should be equal to that removed through vitreous turnover in order to maintain a steady state of drug concentration. Thus, the amount of drug released from silicon diatoms microcarriers can be maintained within the therapeutic window throughout the treatment period, considering the low turnover rate of vitreous humor.[48,49]

2.4. Self-Reporting Capabilities of Silicon Diatoms

Self-reporting drug carriers are highly desirable in drug delivery as they make it possible to monitor the release of drug from the therapeutic formulation by simple visual observation, which is especially relevant for ocular treatments. Our silicon diatom replicas display another interesting properties such as red luminescence when excited under confocal microscopy at 458 nm (**Figure 5**,**6**). A single emission peak in the red region (i.e., 682 nm) is observed from silicon diatoms, which after DNR-loading show two characteristic emission peaks in their photoluminescence (PL) spectrum (Figure 5b). The peak at 594 nm (i.e., green region) is associated with intrinsic luminescence of DNR molecules and at 682 nm (i.e., red region) is due to the intrinsic luminescence of silicon diatoms. After 5 days of release, we found out that the intensity of the first peak (i.e., DNR peak) decreased, while the intensity of the PL peak associated with silicon diatoms was almost constant throughout. This trend was further validated by measuring the PL spectrum of these drug-loaded microstructures after 30 days (Figure 5b). The obtained results denote that the PL peak associated with the intrinsic luminescence of silicon diatoms is predominant at this stage of the release as compared to that of DNR, which is almost attenuated due to the release of DNR molecules. Therefore, the presence of two characteristic PL peaks at different wavelengths enables a precise monitoring of the drug release, the different stages of which can be easily established without interference between the characteristic luminescence peaks of the drug and the carrier. The results are

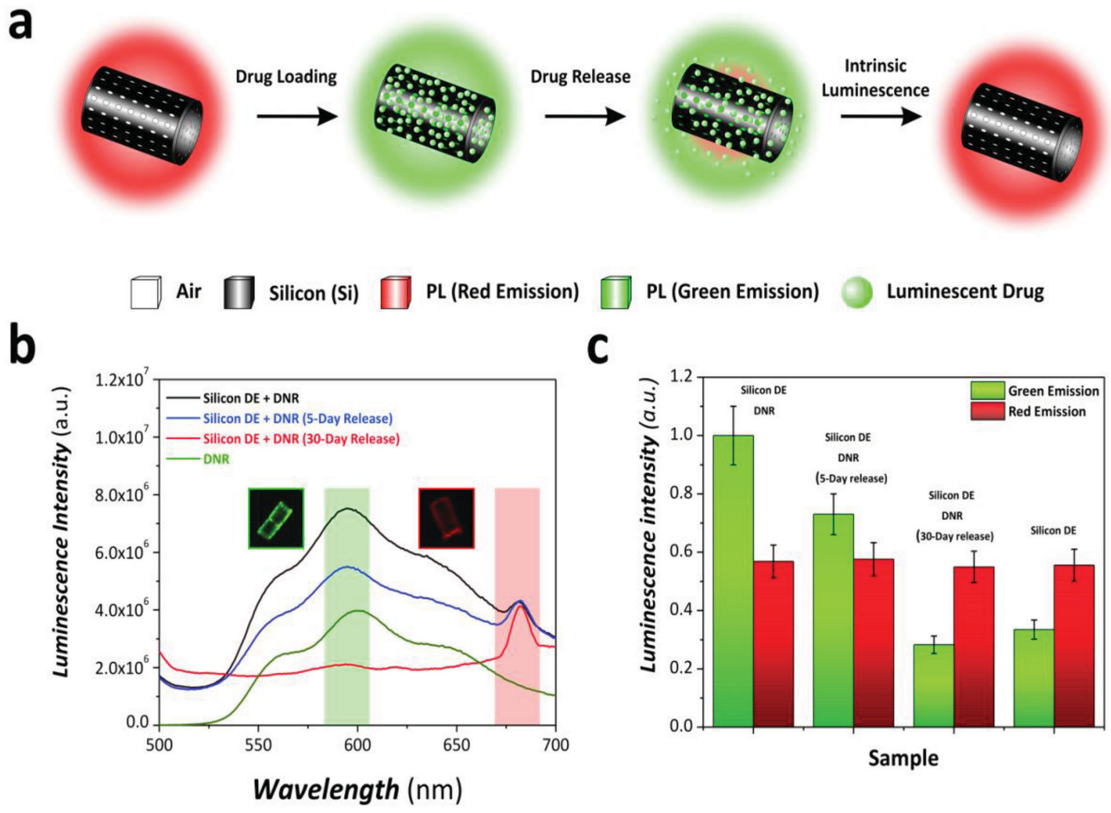

Figure 5. Demonstration of the self-reporting capability of silicon diatom microcarriers for spectroscopic monitoring of the release of luminescent drugs. a) Schematic illustration showing DNR loading onto silicon diatom and the change in luminescence at the different stages of the release process. b) Obtained photoluminescence spectra after 5 and 30 days of DNR release showing two peaks at 594 nm (i.e., green region) are associated with luminescence of DNR molecules and at 682 nm (i.e., red region) are due to the intrinsic luminescence of silicon diatoms. Corresponding confocal microscope images in the green (594 nm) and red (682 nm) regions are presented in the inset. c) Bar-chart showing the intensity of luminescence measured from confocal microscope images after the different stages of the drug-releasing process.

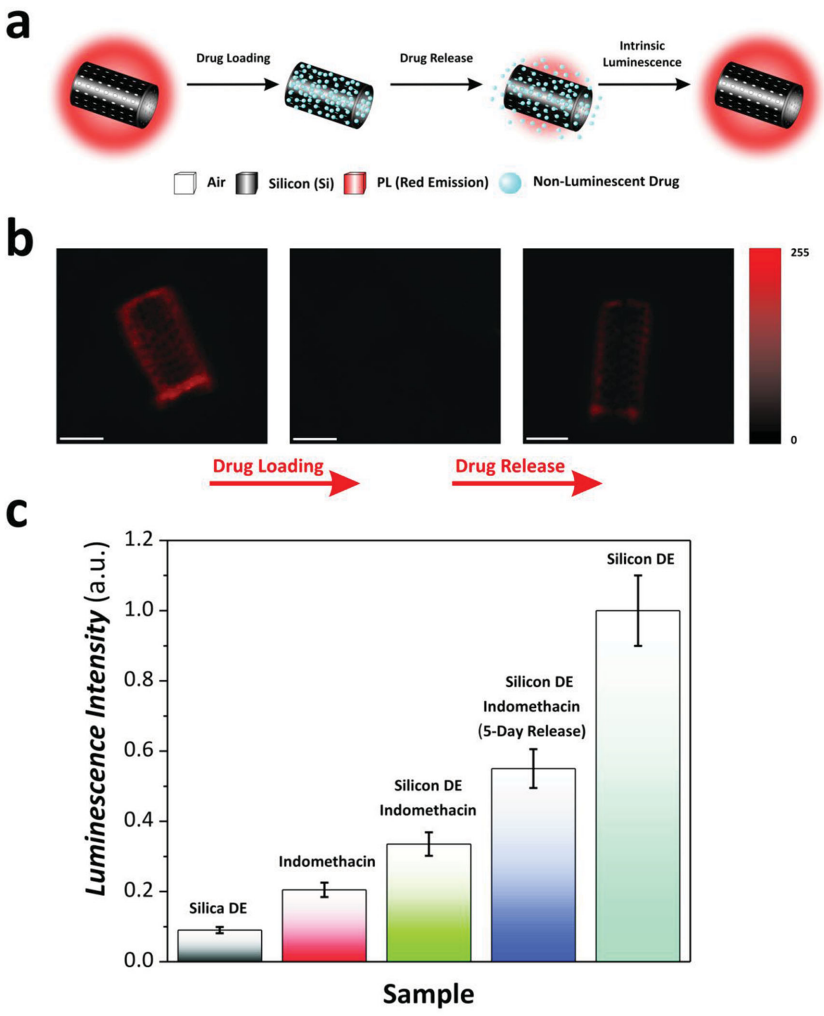

Figure 6. Evaluation of the self-reporting capability of silicon diatom microcarriers for monitoring the release of nonluminescent drugs. a) Schematic illustration showing nonluminescent drug (indomethacin) loading onto silicon diatoms and the change in luminescence at the different stages of the release process. b) Confocal microscopy images of silicon diatoms under different conditions (from left to right): as-produced (extensive luminescence), after loading with indomethacin (luminescence disappeared), and after 5 d of indomethacin release in elution medium (luminescence returned but with lower intensity). The scale bars for images are 5 μm. c) Bar-chart showing the intensity of luminescence emission at 682 nm during the different stages of the loading and release process.

consistent with fluorescence intensity data obtained through analysis of confocal microscopy images (Figure 4c) confirming the capability of silicon diatoms microcapsules to be used as self-reporting drug carriers for direct monitoring of drug release (e.g., ocular treatment).

We further explored this property by using the quenching of the intrinsic luminescence of silicon diatoms when combined with nonluminescent therapeutics. To this end, we used a nonluminescent model drug, indomethacin (Ind). As Figure 5 shows, the intrinsic luminescence of silicon diatoms was completely quenched after indomethacin loading. However, the luminescence from the silicon diatoms rises progressively as indomethacin is eluted (Figure 5b,c). The whole process was also monitored using PL spectroscopy (Figure S7, Supporting Information), and the results are in good agreement with confocal microscopy observations. Note that this is an important and unique feature of the proposed microcarriers, which can be used to treat some diseases such as exudative ARMD, which is typically treated by intravitreal injections of anti-vascular endothelial growth factor (anti-VEGF) agents and other therapeutics such as triamcinolone, which are nonluminescent drugs. Therefore, the self-reporting property of silicon diatoms based on PL excited with blue light (i.e., 458 nm), which causes no harm to retina, is unique and can be used to precisely monitor the release of luminescent and nonluminescent therapeutics by visual analysis. In conclusion, silicon diatoms provide a more reliable means of monitoring the release of drug in vivo than pSi nanoparticles, the self-reporting capabilities of which are limited by the angle-of-observation dependence.

3. Conclusion

In summary, the development of new self-reporting drug microcarriers based on degradable and luminescent silicon with 3D biologically derived morphology from diatoms is reported. The conversion of silica shell (frustules) of single-cell algae diatoms into silicon diatoms retaining their unique porous structure and their cylindrical morphology using gas-solid displacement method is demonstrated. It was found that the surface area of silicon diatom replicas is significantly increased (10×) compared with pristine diatoms which is explained by volume reduction of building blocks (silica nanoparticles) of silica shell during the conversion process of SiO_2 to Si. In addition, prepared silicon diatoms exhibited high crystallinity and improved degradation rates compared to its silica precursor. The in vitro study of daunorubicin loaded into silicon diatoms showed a prolonged and sustained release for up to 30 days which confirms their capability to be applied as carrier for drug delivery applications and for the prevention of proliferative vitreoretinopathy. The release mechanism was found to be dependent on the diffusion of drug molecules from the nanoporous diatom structure and also on the degradation of the silicon structure itself. In addition, this study demonstrated for the first time that silicon diatoms could act as self-reporting carriers for monitoring the release of luminescent and nonluminescent drugs by simple visual analysis. These results confirm that silicon diatom-based microcarriers are a potential alternative to current clinical therapies used to treat a broad range of ocular diseases, including PVR, CNV in ARMD. Considering their unique biologically shape optimized

for movement in a complex biological environment and their hollow and microcapsule structure silicon diatoms are ideal for designing advanced microcarriers for drug delivery applications for broad medical therapies including theranostics and guided microrobotic devices. Furthermore, silicon diatoms can be obtained from inexpensive and available natural resources (fossilized Diatomaceous Earth) using scalable conversion process, and present a promising alternative to existing synthetic silica and polymer materials.

4. Experimental Section

Materials and Chemicals: Raw unprocessed diatomaceous earth (DE) rocks were provided by Mount Sylvia Pty. Ltd. (Queensland, Australia). The purified form of silica diatoms frustules (silica diatoms) was prepared through multiple purification and isolation steps as described elsewhere.[18] Daunorubicin hydrochloride (DNR), Indomethacin (Ind), and phosphate-buffered saline (PBS) tablets were purchased from Sigma-Aldrich (Australia). Magnesium powder, hydrochloric acid (HCl), and nitric acid (HNO_3) were purchased from Chem-Supply (Australia). All chemicals and reagents were used as-received without further purification steps. Aqueous solutions used in this study were prepared with high purity water Option Q-Purelabs (Australia) (18.2 MΩ).

Preparation of Silicon from Silica Diatoms: Silicon diatoms were prepared by magnesiothermic reduction reaction of silica diatoms supplied from purified and classified DE materials composed of unbroken frustules according to a previously reported process.[39] Briefly, a specific weight ratio of purified silica diatoms to magnesium turnings (reducing agent) (1:1.25 w:w) was evenly placed in a ceramic boat following a layered bed form distribution (i.e., first Mg turnings layer at the bottom and then a silica frustules layer on its top). After that, the boat loaded with silica diatoms and Mg reducing agent was placed in a tubular furnace equipped with a quartz tube (Brother Furnace Co., LTD, China) and the system was heated up to 650 °C at a rate of 10 °C min^{-1} and kept at this temperature for 6 h under constant flow of industrial grade argon gas (99.995%). Subsequently, the samples were left to cool down to room temperature under constant flow of argon gas overnight. The reaction product (dark brown in color) was immersed in HCl (1 M) for 4 h in order to dissolve the side product (i.e., MgO). Next, samples were centrifuged (Sigma 3-30KS, Germany) at 13 000 rpm for 10 min and washed five times with high purity water and once with ethanol. The final washed product was then dried in a vacuum oven (VO 400, Memmert GmbH, Freiburg, Germany). All the silicon diatom samples were stored under vacuum till further use in order to prevent them from oxidation.

Characterizations: Silica diatoms, intermediate product (containing MgO), and silicon diatom replicas were characterized using various analytical techniques including scanning electron microscopy (SEM, FEI Quanta 450 FEG-SEM, USA), energy-dispersive X-ray spectroscopy (EDX), X-ray diffraction (XRD, Rigaku MiniFlex 600, Japan), Fourier transform IR (FTIR) spectroscopy (NicoLET 6700 Thermo Fisher, Australia), Raman spectroscopy (LabRAM HR, JOBIN YVON, Japan), N_2 adsorption–desorption isotherms (Belsorp max, BEL, JAPAN), confocal microscopy (Leica SP5 Spectral Scanning Confocal Microscope), atomic force microscopy (AFM, NT-MDT Ntegra Solaris Atomic Force Microscope), and fluorescence spectroscopy (Fluoromax-4 Horiba Jobin Yvon, Japan, equipped with a Xe lamp used as the excitation light source at room temperature). Detailed information about the experimental conditions for each technique is provided in the Supporting information.

In Vitro Degradation of Silica Diatoms and Silicon Diatom Replicas: The degradation behavior of silica diatoms and silicon diatom replicas was tested in PBS at pH 7.4. This set of experiments aimed to determine how the reduction process could affect the degradation behavior of the different forms of diatoms. Samples (2 mg) of silica diatoms and their silicon replicas were dispersed in eppendorf tubes containing 1.2 mL of PBS. These tubes were placed in a shaking water bath (Ratek instruments PTY LTD, Australia) at 50 rpm and 37 °C for 30 days. Note that these conditions, which simulated real body conditions in terms of temperature and dynamicity, were chosen to gain a more realistic insight into the degradation kinetics of these microstructures as a function of their chemical composition. At predetermined time intervals, the samples were centrifuged at 13 000 rpm for 10 min and supernatant (1 mL) was removed for analysis and replaced by fresh buffer solution to maintain perfect sink conditions throughout.[50] PBS kept under the same conditions was used as a blank. All samples were stored at 4 °C till analysis. Inductively coupled plasma mass spectrometry (ICP-MS, Agilent 7500cs, USA) was used for quantifying the total amount of silicon dissolved during the experiment. A calibration curve was obtained by measuring standard silicon solutions of controlled concentrations with ICP-MS. All samples were diluted 100 times with 2% HNO3 and then filtered with a 0.22 μm Millipore filter prior to analysis.

Drug Loading onto Silica and Silicon Diatoms: In order to load DNR onto silica and silicon diatoms particles, DNR solution (100 μL of 5 mg mL^{-1}) were added to either silica diatoms or silicon diatom replicas (10 mg) suspended in PBS (500 μL) in 1.5 mL eppendorf tubes. The particles were then vortexed for 2 h at room temperature, washed three times with ultrapure water till the solution became colorless, which indicated that all loosely attached drug molecules on the surface were completely removed. The supernatant and the washing solutions were collected for the determination of the total amount of drug loaded. The resulting particles were then dried under vacuum and stored at 4 °C till further use. The amount of drug loaded per each milligram of particles was calculated by Equation (1)

$$m_{\text{Load}} = (m_{\text{T-fed}} - m_{\text{T-left}})/m_{\text{T-DE}} \quad (1)$$

where m_{Load} is the total amount of drug loaded, $m_{\text{T-fed}}$ is the total amount of drug fed, $m_{\text{T-left}}$ is the total amount of drug left in the solution, and $m_{\text{T-DE}}$ is the total amount of diatoms particles.

In Vitro Drug Release: The drug release performance from silica diatoms and silicon diatom replicas was assessed by immersing drug-loaded particles (2 mg of either silica diatoms or silicon diatom replicas) in PBS (1.2 mL) in eppendorf tube at 37 °C. The supernatant (1 mL) was collected for analysis after predetermined time intervals by centrifugation at 13 000 rpm for 10 min. An equal amount of fresh medium was added in order to keep the system under perfect sink conditions. The amount of DNR released was determined by photoluminescence (PL) spectroscopy, exciting the samples at 470 nm and measuring the emission intensity at 590 nm. The concentration of drug was calculated using a standard calibration curve obtained by measuring the fluorescence intensity of known concentrations of DNR. Blank samples were prepared by placing the same amount (2 mg) of empty (i.e., nondrug-loaded) silica diatoms or silicon diatom replicas in PBS under the same conditions. All the aforementioned experiments were repeated three times using freshly prepared samples and averages and standard deviations were estimated.

Self-Reporting Characteristics of Silicon Diatoms: The self-reporting capability of silicon diatoms replicas was studied through a series of experiments with luminescent and nonluminescent model drugs. First, the release of a luminescent drug, DNR, was monitored by recording the PL spectra of silicon diatoms before loading, after DNR loading, 5 days after release, and at the end of the release experiment (i.e., 30 days). Confocal microscopy images were also recorded and the fluorescence intensity of each image was established using ImageJ (public domain program developed at the RSB of the NIH). Next, to gain insight into the self-reporting capabilities of silicon diatoms, this property was further validated by measuring the release of a nonluminescent drug (i.e., indomethacin) though quenching of the intrinsic luminescence of silicon diatom replicas. PL measurements were carried out before and after drug loading and also 5 days after immersion of the silicon diatoms in water to release the loaded indomethacin. PL spectra were recorded with blue light excitation at 458 nm. Likewise in the case of DNR, confocal microscopy was used to visualize the luminescence

quenching from silicon diatoms loaded with indomethacin within the same timeframe.

Supporting Information

Supporting Information is available from the Wiley Online Library or from the author.

Acknowledgements

This research was supported in part by a predoctoral fellowship from the Egyptian Ministry of Higher Education awarded to Shaheer Maher. The authors acknowledge financial support from the Australian Research Council (ARC) through grant numbers DP120101680, FT110100711, and DE140100549 and from the School of Chemical Engineering, The University of Adelaide. The authors thank Mount Sylvia Pty. Ltd. for providing DE material. The authors also thank Soundarrajan Chandrasekaran from University of South Australia for initial help in performing silica conversion experiment, Dr. Lucas Johnson for help in preforming BET experiments, Dr. Diana Tran for SEM imaging, and the Adelaide Microscopy Centre for FEG-SEM characterization.

Received: March 28, 2015
Published online: July 14, 2015

[1] O. C. Farokhzad, R. Langer, *Adv. Drug Delivery Rev.* **2006**, *58*, 1456.
[2] A. A. Manzoor, L. H. Lindner, C. D. Landon, J. Y. Park, A. J. Simnick, M. R. Dreher, S. Das, G. Hanna, W. Park, A. Chilkoti, G. A. Koning, T. L. Ten Hagen, D. Needham, M. W. Dewhirst, *Cancer Res.* **2012**, *72*, 5566.
[3] A. Sharma, U. S. Sharma, *Int. J. Pharm.* **1997**, *154*, 123.
[4] C. Li, S. Wallace, *Adv. Drug Delivery Rev.* **2008**, *60*, 886.
[5] G. A. Hughes, *Nanomed. Nanotechnol. Biol. Med.* **2005**, *1*, 22.
[6] N. Doshi, S. Mitragotri, *Adv. Funct. Mater.* **2009**, *19*, 3843.
[7] J. A. Champion, Y. K. Katare, S. Mitragotri, *J. Controlled Release* **2007**, *121*, 3.
[8] J. A. Champion, S. Mitragotri, *Proc. Natl. Acad. Sci. U.S.A.* **2006**, 103.
[9] P. Thomas, *Bacteria and Viruses*, Lucent Books, Farmington Hills, MI **2004**.
[10] S. E. A. Gratton, P. A. Ropp, P. D. Pohlhaus, J. C. Luft, V. J. Madden, M. E. Napier, J. M. Desimone, *Proc. Natl. Acad. Sci. U.S.A.* **2008**, 105.
[11] D. Dendukuri, D. C. Pregibon, J. Collins, T. A. Hatton, P. S. Doyle, *Nat. Mater.* **2006**, 5.
[12] D. Losic, J. G. Mitchell, N. H. Voelcker, *Adv. Mater.* **2009**, *21*, 2947.
[13] M. Sumper, E. Brunner, *Adv. Funct. Mater.* **2006**, *16*, 17.
[14] H. E. Townley, A. R. Parker, H. White-Cooper, *Adv. Funct. Mater.* **2008**, *18*, 369.
[15] R. Gordon, D. Losic, M. A. Tiffany, S. S. Nagy, F. A. S. Sterrenburg, *Trends Biotechnol.* **2009**, *27*, 116.
[16] J. T. Chao, M. J. Biggs, A. S. Pandit, *Expert Opin. Drug Delivery* **2014**, *11*, 1687.
[17] D. Losic, Y. Yu, M. S. Aw, S. Simovic, B. Thierry, J. Addai-Mensah, *Chem. Commun.* **2010**, *46*, 6323.
[18] M. S. Aw, S. Simovic, J. Addai-Mensah, D. Losic, *Nanomedicine* **2011**, *6*, 1159.
[19] M. Bariana, M. S. Aw, D. Losic, *Adv. Powder Technol.* **2013**, *24*, 757.
[20] Y. Yang, A.-M. Jonas, L. Dusan, *Sci. Technol. Adv. Mater.* **2012**, *13*, 015008.
[21] T. Kumeria, M. Bariana, T. Altalhi, M. Kurkuri, C. T. Gibson, W. Yang, D. Losic, *J. Mater. Chem. B* **2013**, *1*, 6302.
[22] M. S. Aw, M. Bariana, Y. Yu, J. Addai-Mensah, D. Losic, *J. Biomater. Appl.* **2013**, *28*, 163.
[23] Y. E. Choonara, V. Pillay, M. P. Danckwerts, T. R. Carmichael, L. C. Du Toit, *J. Pharm. Sci.* **2010**, *99*, 2219.
[24] J. Chhablani, A. Nieto, H. Hou, E. C. Wu, W. R. Freeman, M. J. Sailor, L. Cheng, *Invest. Ophthalmol. Vis. Sci.* **2013**, *54*, 1268.
[25] R. D. Jager, L. P. Aiello, S. C. Patel, E. T. Cunningham, *Retina* **2004**, *24*, 676.
[26] K. I. Hartmann, A. Nieto, E. C. Wu, W. R. Freeman, J. S. Kim, J. Chhablani, M. J. Sailor, L. Cheng, *J. Ocul. Pharmacol. Ther.* **2013**, *29*, 493.
[27] S. Näkki, J. Rytkönen, T. Nissinen, C. Florea, J. Riikonen, P. Ek, H. Zhang, H. A. Santos, A. Närvänen, W. Xu, V.-P. Lehto, *Acta Biomater.* **2015**, *13*, 207.
[28] J. Hernandez-Montelongo, N. Naveas, S. Degoutin, N. Tabary, F. Chai, V. Spampinato, G. Ceccone, F. Rossi, V. Torres-Costa, M. Manso-Silvan, B. Martel, *Carbohydr. Polym.* **2014**, *110*, 238.
[29] H. J. Lee, Y. Son, D. Kim, Y. K. Kim, N. Choi, E.-S. Yoon, I.-J. Cho, *Sens. Actuators, B* **2015**, *209*, 413.
[30] F. Peng, Y. Su, X. Ji, Y. Zhong, X. Wei, Y. He, *Biomaterials* **2014**, *35*, 5188.
[31] H. Jaganathan, B. Godin, *Adv. Drug Delivery Rev.* **2012**, *64*, 1800.
[32] D. Fan, E. De Rosa, M. B. Murphy, Y. Peng, C. A. Smid, C. Chiappini, X. Liu, P. Simmons, B. K. Weiner, M. Ferrari, E. Tasciotti, *Adv. Funct. Mater.* **2012**, *22*, 282.
[33] S. P. Low, K. A. Williams, L. T. Canham, N. H. Voelcker, *Biomaterials* **2006**, *27*, 4538.
[34] Y. Koh, S. Jang, J. Kim, S. Kim, Y. C. Ko, S. Cho, H. Sohn, *Colloids Surf., A* **2008**, *313–314*, 313.
[35] S. Koynov, R. N. Pereira, I. Crnolatac, D. Kovalev, A. Huygens, V. Chirvony, M. Stutzmann, P. De Witte, *Adv. Eng. Mater.* **2011**, 13.
[36] J. Diener, Y. R. Shen, D. I. Kovalev, G. Polisski, F. Koch, *Phys. Rev. B* **1998**, 58.
[37] J. R. Dorvee, A. M. Derfus, S. N. Bhatia, M. J. Sailor, *Nat. Mater.* **2004**, 3.
[38] J. Toster, I. Kusumawardani, E. Eroglu, K. S. Iyer, F. Rosei, C. L. Raston, *Green Chem.* **2014**, *16*, 82.
[39] S. Chandrasekaran, M. J. Sweetman, K. Kant, W. Skinner, D. Losic, T. Nann, N. H. Voelcker, *Chem. Commun.* **2014**, *50*, 10441.
[40] Z. Bao, M. R. Weatherspoon, S. Shian, Y. Cai, P. D. Graham, S. M. Allan, G. Ahmad, M. B. Dickerson, B. C. Church, Z. Kang, H. W. Abernathy Iii, C. J. Summers, M. Liu, K. H. Sandhage, *Nature* **2007**, *446*, 172.
[41] C. E. Hamm, R. Merkel, O. Springer, P. Jurkojc, C. Maier, K. Prechtel, V. Smetacek, *Nature* **2003**, *421*, 841.
[42] Z. Bao, E. M. Ernst, S. Yoo, K. H. Sandhage, *Adv. Mater.* **2009**, 21.
[43] P. M. Dove, N. Han, A. F. Wallace, J. J. De Yoreo, *Proc. Natl. Acad. Sci. U.S.A.* **2008**, *105*, 9903.
[44] P. Wiedemann, R. D. Hilgers, P. Bauer, K. Heimann, *Am. J. Ophthalmol.* **1998**, *126*, 550.
[45] A. Sadaka, G. P. Giuliari, *Clin. Ophthalmol.* **2012**, *6*, 1325.
[46] P. Wiedemann, N. Sorgente, C. Bekhor, R. Patterson, T. Tran, S. J. Ryan, *Invest. Ophthalmol. Vis. Sci.* **1985**, *26*, 719.
[47] K. Nan, F. Ma, H. Hou, W. R. Freeman, M. J. Sailor, L. Cheng, *Acta Biomater.* **2014**, *10*, 3505.
[48] I. Fatt, *Bull. Math. Biol.* **1975**, *37*, 85.
[49] U. B. G. Laurent, J. R. E. Fraser, *Exp. Eye Res.* **1983**, *36*, 493.
[50] M. Gibaldi, S. Feldman, *J. Pharm. Sci.* **1967**, *56*, 1238.